Inorganic Chemistry

Article

pubs.acs.org/IC

Iron(III) Complexes with Meridional Ligands as Functional Models of Intradiol-Cleaving Catechol Dioxygenases

Tünde Váradi,[†] József S. Pap,[†] Michel Giorgi,[‡] László Párkányi,[§] Tamás Csay,[#] Gábor Speier,[†] and József Kaizer*,[†]

[†]Department of Chemistry, University of Pannonia, 8201 Veszprém, Hungary

[‡]Aix-Marseille Université, FR1739, Spectropole, Campus St. Jérôme, Avenue Escadrille Normandie-Niemen, 13397 Marseille cedex 20, France

[§]Chemical Research Center, Hungarian Academy of Sciences, 1525, Budapest, Hungary

[#]Radiation Chemistry Department, Centre for Energy Research, Hungarian Academy of Sciences, 1121 Budapest, Hungary

S Supporting Information

ABSTRACT: Six dichloroiron(III) complexes of 1,3-bis(2′-arylimino)isoindoline (BAIH) with various N-donor aryl groups have been characterized by spectroscopy (infrared, UV–vis), electrochemistry (cyclic voltammetry), microanalysis, and in two cases X-ray crystallography. The structurally characterized $Fe^{III}Cl_2(L^n)$ complexes (n = 3, L^3 = 1,3-bis(2′-thiazolylimino)-isoindoline and n = 5, L^5 = 1,3-bis(4-methyl-2′-piridylimino)isoindoline) are five-coordinate, trigonal bipyramidal with the isoindoline ligands occupying the two axial and one equatorial positions meridionally. These compounds served as precursors for catechol dioxygenase models that were formed in solution upon addition of 3,5-di-*tert*-butylcatechol (H_2DBC) and excess triethylamine. These adducts react with dioxygen in *N*,*N*-dimethylformamide, and the analysis of the products by chromatography and mass spectrometry showed high intradiol over extradiol selectivity (the intradiol/extradiol product ratios varied between 46.5 and 6.5). Kinetic measurements were performed by following the change in the intensity of the catecholate to iron ligand-to-metal charge transfer (LMCT) band, the energy of which is influenced by the isoindolinate-ligand (827–960 nm). In combination with electrochemical investigations the kinetic studies revealed an inverse trend between reaction rates and oxidation potentials associated with the coordinated DBC^{2-}. On the basis of these results, a substrate activation mechanism is suggested for this system in which the geometry of the peroxide-bridged intermediate may be of key importance in regioselectivity.

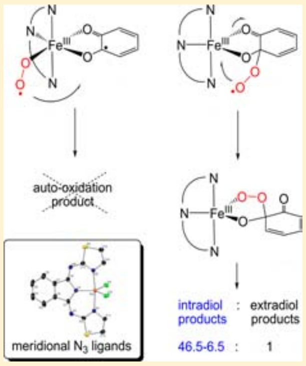

■ INTRODUCTION

Most soil bacteria are able to use aromatic compounds either from natural or anthropogenic sources as their sole carbon and energy source. They utilize molecular oxygen to cleave aromatic rings in multistep processes that are dependent on dioxygenase enzymes.[1−3] This capability has attracted much attention because the conversion of aromatics to water-soluble aliphatic products in the environment is a desirable goal in areas of bioremediation and environmental microbiology.[4] The most thoroughly studied reaction is perhaps the ring cleavage of 1,2-dihydroxybenzene (catechol) that is catalyzed by nonheme, iron-dependent catechol dioxygenase enzymes.[3,5,6] Two classes are distinguished by their regioselectivity: the intradiol catechol dioxygenases cleave the bond between the enediol carbons whereas the extradiol enzymes do so at the adjacent carbon−carbon bond.[3,6] X-ray structural analysis of intradiol-cleaving enzymes, for example those of the protocatechuate 3,4-dioxygenase (3,4-PCD) from *Pseudomonas* species, concluded that the iron(III) center is trigonal-bipyramidal coordinating four protein ligands (2-histidine-2-tyrosine motif) and one hydroxide[7−9] (Scheme 1), a highly different binding site from the 2-histidine-1-carboxylate facial triad motif found in iron(II)-dependent extradiol-cleaving enzymes.[6,10]

Scheme 1. Schematic Structure of the Active Site in the Intradiol- (Left) and Extradiol-Cleaving (Right) Catechol Dioxygenase Enzymes

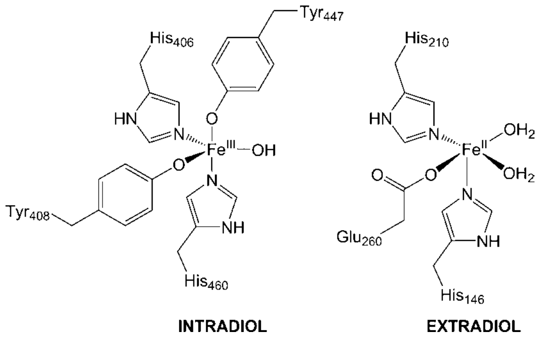

Received: November 7, 2012
Published: January 15, 2013

The known structure in combination with spectroscopic studies has led to a generally accepted substrate activation mechanism for the intradiol enzymes[11] (Scheme 2). According to this mechanism, one proton is abstracted from the catechol substrate by the hydroxide ligand, the second by a tyrosyl ligand, and upon formation of the substrate-enzyme adduct the tyrosine ligand and the water molecule leave the coordination sphere. The five-coordinate structure of the remaining adduct has been shown.[12] In the adduct the substrate is thought to have considerable semiquinonate radical character that can be attacked by dioxygen to form an alkylperoxo intermediate (some authors did not exclude initial attack of dioxygen at the iron, preceding the closure of the peroxo-bridge[13]). It should be noted that the alkyl(hydro)peroxo-iron species is an intermediate currently canonized for both the intra- and the extradiol-cleaving catalytic cycle, the only difference is in the oxidation state of the iron center (iron(III) for intradiol vs iron(II) for extradiol).[11,14] However, a very recent density functional study debates the unchanged iron(II) oxidation state in the extradiol catalytic cycle; instead it predicts an iron(III)-superoxo reactive species that directly attacks the substrate.[15] Experimental evidence shows that the superoxo species can be formed in the reaction of enzyme−substrate complexes with O_2, but the formation of the reactive species requires subsequent electron transfer from the catechol to the metal.[16−19]

Scheme 2. Proposed Reaction Mechanism for the Intradiol-Cleaving Enzyme[a]

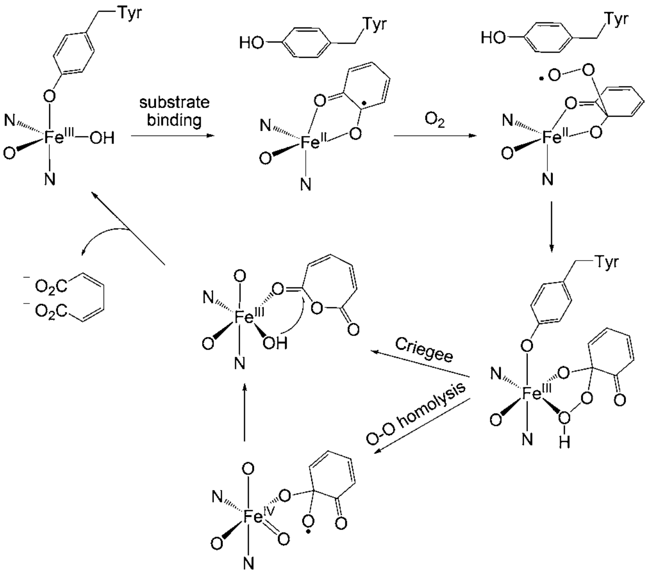

[a]Key steps have been selected to illustrate the discussion in the text.

Although computational studies are ahead of the experimental investigations with respect to active intermediates, it can be stated that the regioselectivity of the intradiol-cleaving enzymes and models can be primarily attributed to the higher Lewis acidity of the iron(III) center that enhances the covalency in the substrate-iron complex by lowering the energy of the lowest unoccupied molecular orbital (LUMO) of the iron site. It was also supposed that the higher oxidation state of iron assists the "1,2-acyl migration" by promoting the homolysis of the O−O bond[11] and may stabilize a proposed oxoiron(IV) species that is thereby formed (Scheme 2). In contrast, regarding the extradiol enzymes, stereoelectronic positioning of the hydroperoxide group relative to the cyclohexadienone ring seems to be required to promote "1,2-alkenyl migration", in combination with acid−base catalysis by active-site residues.[11,20−22]

In their recent computational studies on the intradiol-cleaving enzyme, Borowski and Siegbahn[23] highlighted the significance of the in-plane geometry of the peroxo intermediate. According to their results the peroxo species undergoes a geometric transition that allows an X−OH moiety (H_2O or Tyr447) to occupy the axial position but also changes the dihedral angle defined by the peroxo oxygens (O1 and O2) and the C4 and C3 carbons in the substrate ring from −76° to −170°. This planar geometry is retained in the next steps, where the protonation of the peroxo-bridge takes place. They claim that this arrangement is pivotal for the progress of the catalytic cycle as this makes the Criegee 1,2-rearrangement (involving the simultaneous cleavage of the O1−O2 and C3−C4 bonds concerted with formation of a bond between O2 and O3) viable. Their spin density calculations suggested that the direct Criegee 1,2-rearrangement should be *heterolytic* with an OH^- leaving group and a formal O^+ inserted into the C4−C3 bond, dominating the alternative *homolytic* O−O bond cleavage pathway, both leading to muconic anhydride. However, the *homolytic* pathway was also shown to be viable by Xin and Bugg[11] using mechanistic probes. Their results support that the "acyl migration" is best described as the *homolytic* dissociation of the O−O bond leading to an iron(IV) species and an alkoxyl radical, in accordance with the lack of additional acid−base residues in the intradiol dioxygenase active site.

Our recent state of understanding indicates that the fine details of either the extradiol- or the intradiol-cleaving reaction are still elusive, and in addition to the numerous artificial iron model complexes[24−37] new model studies can be still informative. As Xin and Bugg frames it: "...further modeling studies on these mechanisms might reveal the effects that the precise geometry of the hydroperoxide complex and the positioning of active site residues have on the O−O homolysis versus Criegee rearrangement pathways".[11] Previous model studies demonstrated the effect of Lewis acidity on reaction rates,[38] but other factors, such as steric hindrance at the iron center,[25,27,39,40] asymmetry in substrate binding,[41,42] combined solvent/ligand effects,[27,36] stereoelectronic effects[31,43] and spin transition at the metal site[44] have been also addressed as of potentially general importance in reactivity.

Models applying N_4 ligands (Scheme 3) were shown to produce intradiol products very selectively, which was attributed to the enzyme-like substrate activation mechanism[45−47] (e.g., no vacant site for O_2 binding). In a more recent study, however, the regioselectivity with N_4 ligands was driven by the amount of added base:[30] extradiol products were predominant when only 1 equiv of base was added, while 2 equiv of base led to intradiol products, too. This was explained by means of the protonation and subsequent dissociation of a pyridyl pendant-arm when less base was added to facilitate O_2 binding at the iron(III) center. Similarly, the ethoxyl arm of *N*,*N*-bis(2-pyridylmethyl)-*N*-(2-hydroxyethyl)amine (Scheme 3)[28] was claimed to be capable of accepting the proton from the catechol substrate thus functioning as internal base. These ligands are therefore good mimics for the internal base-effect that operates in the substrate binding process.

Tridentate ligands have been widely used in intradiol model studies. The octahedral $Fe^{III}Cl(L)(S)$ complexes are usually

Scheme 3. Some Ligands Used in Recent Model Complexes for Catechol Dioxygenase Enzymes

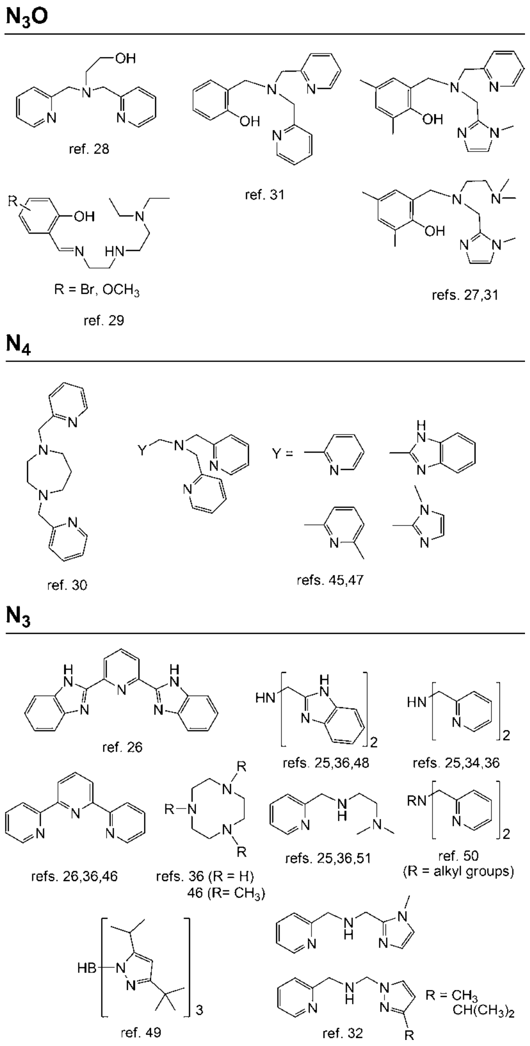

generated in situ from octahedral $Fe^{III}Cl_3(L)$ precursors by adding base. Regiospecifity is largely determined by the geometry of the ligands. Selectivity is shifted toward intradiol-cleavage when meridional N_3 geometry[26,36,46] is available (or forced by the ligand), whereas facial coordination of the supporting ligand leads to extradiol-cleavage.[34,36,46,49−51] While numerous flexible, linear N_3 ligands have been used in model complexes in the literature,[24,25,32,34,36,48,50,51] to our knowledge only a few meridional examples were studied.[26,36,46] In these studies the iron(III) precursor complexes are generally octahedral with three chlorides residing in the coordination sphere that leaves one chloride in the substrate-iron adduct complex thus complicating the dioxygen-binding step in the mechanism.

Recently, we synthesized biomimetic complexes with relatively rigid, tridentate N_3 donor isoindoline-based ligands.[52−56] New members of this ligand family became available by introducing different groups at the imine functions as illustrated in Scheme 4. Earlier, we reported the structure of $FeCl_2(L^4)$, a trigonal bipyramidal iron(III) complex.[57] Such five-coordinate compounds with the obtained ligand variations offered the chance to investigate catechol dioxygenase model complexes using 3,5-di-*tert*-butylcatechol (H_2DBC) as model substrate. Therefore we synthesized the analogues of $FeCl_2(L^4)$ as precursors for Fe(L)(DBC) enzyme−substrate model complexes. These new models unlike the earlier examples lack the third chloride ligand, and the rigid ligand backbone does not allow significant geometric changes in the coordination sphere. This way it seemed viable to elucidate the role of stereochemical and electronic factors in the enzyme-like reaction. In this paper we discuss the reactivity of the substrate adducts with dioxygen in context with the ligand modifications and redox chemistry.

Scheme 4. Structure of the Isoindoline-Based Ligands Involved in This Study

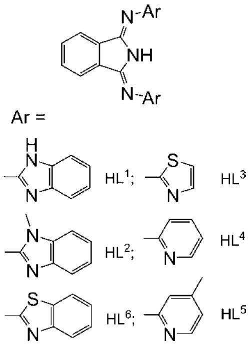

■ EXPERIMENTAL SECTION

Materials. All manipulations were performed under a pure argon atmosphere using standard Schlenk-type inert-gas techniques unless otherwise stated. Solvents used for the reactions were purified by literature methods and stored under argon. The isoindoline-based ligands HL^1-HL^7 have been synthesized according to published procedures.[52,55,56,58,59]

Synthesis and Characterization of the Complexes. Complexes may be synthesized according to the procedure published for $Fe^{III}Cl_2(L^4)$ (**4**).[57] However, in an alternative reaction, where $FeCl_3 \cdot 6H_2O$ was reacted with the appropriate ligand in 1:1 ratio, in refluxing methanol under argon atmosphere the compounds could be obtained with better yields; therefore this method was followed for all compounds.

*$Fe^{III}Cl_2(L^1)$ (**1**).* HL^1 (1.50 g, 4 mmol) and $FeCl_3 \cdot 6H_2O$ (1.08 g, 4 mmol) were refluxed in 30 mL of methanol for 6 h under argon atmosphere. After cooling to room temperature the brown precipitate was filtered off, washed with cold methanol, and dried under vacuum. Yield: 1.44 g (72%). Anal. Calcd. for $C_{22}H_{14}Cl_2FeN_7$: C, 52.52; H, 2.80; N, 19.49. Found: C, 52.7; H, 2.8; N, 19.4%. FT−IR bands (KBr, cm^{-1}): 3330m, 3068w, 1621w, 1572m, 1552s, 1521m, 1431m, 1319w, 1292w, 1076m, 1038m, 757w, 745m, 700w, 598w. UV−vis (DMF) [λ_{max}, nm (log ε)] 288 (4.44), 344 (4.38), 372 (4.36), 403 (4.35), 421 (4.39), 444 (4.27), 500sh (3.61). All complexes were synthesized according to the above procedure.

*$Fe^{III}Cl_2(L^2)$ (**2**).* Yield: 1.47 g (69%). Anal. Calcd. For $C_{24}H_{18}Cl_2FeN_7$: C, 54.27; H, 3.42; N, 18.46. Found: C, 54.2; H, 3.4; N, 18.4%. FT−IR bands (KBr, cm^{-1}): 3052w, 2936w, 1554s, 1504w, 1477m, 1448w, 1400m, 1330m, 1178w, 1050s, 743m, 704w. UV−vis (DMF) [λ_{max}, nm (log ε)] 292 (4.32), 383 (4.35), 444 (4.14), 479 (3.96), 510sh (3.80).

*$Fe^{III}Cl_2(L^3)$ (**3**).* Yield: 1.15 g (66%). Anal. Calcd. For $C_{14}H_8Cl_2FeN_5S_2$: C, 38.47; H, 1.84; N, 16.22. Found: C, 38.6; H, 1.9; N, 16.4%. FT−IR bands (KBr, cm^{-1}): 3121w, 3103w, 1609w, 1534s, 1503m, 1470w, 1411w, 1326m, 1245m, 1180w, 1153w, 1031s, 873m, 777w, 714s, 638w, 527w. UV−vis (DMF) [λ_{max}, nm (log ε)] 290 (4.18), 348 (4.23), 412 (4.25), 430 (4.29), 454 (4.29), 524sh (3.32). Single crystals for structure determination were grown from a dichloromethane/toluene mixture.

*$Fe^{III}Cl_2(L^4)$ (**4**).*[57] Yield: 1.16 g (68%). Anal. Calcd. For $C_{18}H_{12}Cl_2FeN_5$: C, 50.86; H, 2.85; N, 16.48. Found: C, 51.0; H,

2.9; N, 16.6%. FT−IR bands (KBr, cm^{-1}): 3052w, 1632w, 1601w, 1577s, 1551m, 1530m, 1467s, 1430m, 1268m, 1183m, 1149m, 1050s, 1006w, 832m, 775m, 710m, 693w, 533w, 514w. UV−vis (DMF) [λ_{max}, nm (log ε)] 277 (4.39), 339 (4.23), 356 (4.19), 362sh (4.18), 392 (4.20), 455sh (3.87).

Fe^{III}Cl$_2$(L^5) (5). Yield: 0.87 g (48%). Anal. Calcd. For $C_{20}H_{16}Cl_2FeN_5$: C, 53.01; H, 3.56; N, 15.46. Found: C, 53.2; H, 3.6; N, 15.7%. FT−IR bands (KBr, cm^{-1}): 3044w, 2919w, 1649w, 1611w, 1580s, 1522m, 1471m, 1448w, 1403m, 1353w, 1294w, 1277m, 1234w, 1192m, 1173m, 1043s, 1006w, 938m, 889m, 817m, 777w, 712m, 698w, 521w, 464m. UV−vis (DMF) [λ_{max}, nm (log ε)] 280 (4.09), 296 (4.09), 331 (4.24), 367 (4.26), 386 (4.29), 405sh (4.18), 460sh (3.69). Single crystals for structure determination were grown from a dichloromethane/toluene mixture.

Fe^{III}Cl$_2$(L^6) (6). Yield: 1.15 g (66%). Anal. Calcd. For $C_{22}H_{12}Cl_2FeN_5S_2$: C, 49.18; H, 2.25; N, 13.04. Found: C, 49.0; H, 2.4; N, 12.9%. FT−IR bands (KBr, cm^{-1}): 3053w, 1617m, 1530s, 1477m, 1456m, 1424m, 1318m, 1289m, 1267m, 1255m, 1231m, 1173w, 1072w, 1033s, 804w, 751m, 718m, 653w, 465w. UV−vis (DMF) [λ_{max}, nm (log ε)] 369 (4.09), 389 (4.03), 420 (4.02), 445 (4.16), 474 (4.21), 508 (4.00).

Analytical and Physical Measurements. Infrared spectra were recorded on an Avatar 330 FT-IR Thermo Nicolet instrument. UV−vis spectra were recorded on an Agilent 8453 diode−array spectrophotometer using quartz cells. Microanalyses were done by the Microanalytical Service of the University of Pannonia. Cyclic voltammograms (CV) were taken on a VoltaLab 10 potentiostat with VoltaMaster 4 software for data process. The electrodes were as follows: glassy carbon (working), Pt (auxiliary), and Ag/AgCl in 3 M KCl (reference). The potentials were referenced vs the ferrocene/ferrocenium (Fc/Fc$^+$) redox couple. The crystal evaluation and intensity data collection for **3** was performed on a Bruker−Nonius Kappa CCD single-crystal diffractometer using Mo Kα radiation (λ = 0.71073 Å) at 293(2) K. For **5**·$C_6H_5CH_3$ data collection was performed on a Rigaku R-Axis Rapid single-crystal diffractometer using Mo Kα radiation at 293(2) K. Further experimental details can be found in the Supporting Information, cif file. Structure solution was performed with SHELX-97[60] for **3** or SIR2008[61] for **5**·$C_6H_5CH_3$, and SHELX-97[60] was used for full matrix least-squares refinement on F^2.

Analysis of the Ring-Cleavage Products. Documented procedures[25,26,32,35,36,50,51] were followed to identify the products of the catechol dioxygenase model reactions. The precursor complexes **1**−**6** (0.1 mmol), H_2DBC and 4 equiv of triethyl amine were dissolved in DMF (5 mL), and the mixture was stirred at 60 °C for 48 h. The solvent was then evaporated under vacuum, and the oily residue was treated with 5 mL of 10% sulfuric acid to extract the iron salt. The aqueous mixture was extracted with 3 × 10 mL of diethylether. The extracts were dried over $CaCl_2$, concentrated under vacuum, and the samples were analyzed by GC-MS. The samples were analyzed on a HP 4890D gas chromatograph equipped with a 30 m (Ø = 0.32 mm) HP-1 capillary column, programmed to heat from 50 to 250 °C at a rate of 5 °C/minute. Retention times of the products **A**−**F** (Scheme 6) are listed in Supporting Information, Figure S1 that shows the chromatogram of the sample from **1d**. The elution order for the products was the same as in earlier studies. GC-MS measurements were performed on a HP 5890 gas chromatograph (HP-1 column) connected to a HP 5971A mass selective detector. The samples were also analyzed by LC-MS to check the possible presence of acidic products. To separate the reaction products an Agilent 1200 liquid chromatograph equipped with a 5 mm ×100 mm Phenomenex Kinetex XB-C18 capillary column, particle size 2.6 μm was used. Eluent B, a mixture of degassed acetonitrile with 5% of water and 0.1% of formic acid and eluent A, 0.1% aqueous formic acid, was filtered through a 0.45 μm RC-filter. LC-separations were performed at 25 °C at a flow rate of 0.3 cm^3 min^{-1}. Gradient elution was used with A/B eluent: 0 min 10% B, 3 min 10% B, 10 min 30%, 50 min 50% B. Mass spectrometric detection in electrospray ionization (ESI) positive ionization mode was performed on an Agilent 6410 triple quad mass spectrometer. These LC-MS experiments confirmed the products identified by GC-MS.

Kinetic Measurements. Runs of [Fe(DBC)(L^n)] (n = 1−6, c = 0.5−2 mM) oxygenation were performed in 30 mL of DMF, in reaction vessels open to air and thermostatted to 55−70 (±0.5)°C. Samples (~0.2 mL) were taken for which the electronic absorption spectrum was measured in optical quartz cells (l = 0.1 mm) at appropriate time intervals (2−5 min). The progress of the reaction was followed by detecting the change in intensity of the DBC^{2-} to iron charge transfer band. Dioxygen dependence was determined by mixing O_2 and Ar with the help of a gas buret connected to the reaction vessel, or simply using pure O_2. The volume of O_2 in the gas mixture was in high excess (>100 ×) to the expected maximal dioxygen uptake calculated for complete conversion of the complex. In the case of [Fe(DBC)(L^5)] one experiment was performed by dissolving the solid compound in DMF. (The complex was isolated from a DMF solution as a green-black solid by slow evaporation under a stream of argon gas. FT-IR spectroscopy showed no evidence for the presence of DMF at the sixth coordination site according to the lack of the characteristic ν(C═O) band at ~1630 cm^{-1}. Thus our results support a five-coordinate adduct in the solid state.) The kinetic experiment by dissolving the solid gave similar result to that of the in situ method (Supporting Information, Figure S4).

RESULTS AND DISCUSSION

Solid State Structural Information on the Fe^{III}Cl$_2$(L^n) Complexes (X-ray Crystallography and IR Spectroscopy). Three of the precursor complexes, **3**, **4**,[57] and **5** have been structurally characterized by X-ray crystallography. The molecular structures of the new compounds (**3** and **5**) are shown in Figures 1 and 2. The thermal ellipsoids are drawn at 30% probability. Crystallographic data and details of the structure determination are given in Table 1, and selected bond lengths and angles are listed in Table 2. The geometry of these complexes is best described as distorted trigonal bipyramidal with τ-values[62] of 0.83, 0.86, and 0.77 for **3**, **4**, and **5**, respectively. The isoindoline ligands adopt a meridional topology, the three nitrogen atoms occupying one equatorial and the two apical positions. The central pyrrolic nitrogen (N_{ind}) sits closest to the iron(III) center, while the other two pyridinic (or thiazolic) nitrogen atoms are significantly farther from the metal (the Fe−N_{ind} is 1.963(1) Å, the Fe−N_{py} avg. is 2.148 Å for **4**[57]). This difference may originate from the greater

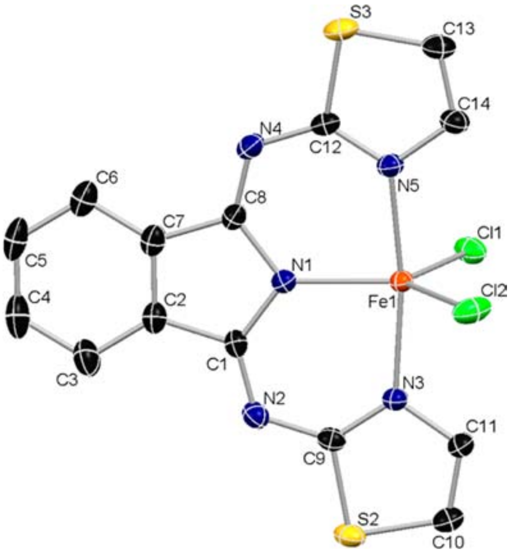

Figure 1. X-ray structure of **3** (hydrogen atoms are omitted for clarity, thermal ellipsoids are plotted at 30% probability).

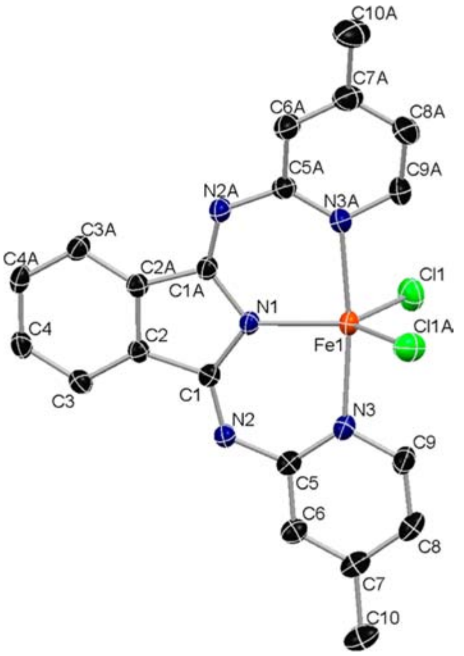

Figure 2. X-ray structure of **5** (hydrogen atoms and the toluene molecule are omitted for clarity, thermal ellipsoids are plotted at 30% probability).

Table 1. Crystal Structure Details for 3 and 5·$C_6H_5CH_3$

	3	5·$C_6H_5CH_3$
chemical formula	$C_{14}H_8Cl_2FeN_5$	$C_{27}H_{24}Cl_2FeN_5$
formula weight	437.12	545.26
space group	triclinic, $P\bar{1}$	triclinic, $P\bar{1}$
a, Å	7.4218(2)	9.6965(14)
b, Å	8.2660(2)	9.9350(14)
c, Å	16.1637(6)	13.7073(16)
α, deg	75.587(1)	101.168(3)
β, deg	88.931(1)	92.163(3)
γ, deg	63.158(1)	91.148(3)
V, Å^3	851.88(4)	1294.1(3)
Z	2	2
D_{calc}, Mg m^{-3}	1.704	1.399
temperature, K	293(2)	293(2)
unique reflections	4165	4358
data > 2σ/parameters/restraints	3393/217/0	3522/319/6
R1^a [$F^2 > 2\sigma(F^2)$], wR2^b (F^2)	0.0405, 0.1095	0.0506, 0.1407
goodness of fit	1.122	1.052

^{a}R1 = $\sum||F_o| - |F_c||/\sum|F_o|$. ^{b}$w$R2 = $[\sum w(F_o^2 - F_c^2)^2/\sum w(F_o^2)^2]^{1/2}$, $w = 1/\sigma^2(F_o)^2 + (AP)^2 + BP$, where $P = [F_o^2 + 2F_c^2]/3$; A = 0.0637 and 0.1052, B = 0.5871 and 0 for **3** and **5**·$C_6H_5CH_3$, respectively.

Lewis basicity of the deprotonated pyrrolic nitrogen. The Fe−Cl distances are all ~2.23 Å (2.224(1) Å and 2.234(1) Å in **4**[57]), somewhat shorter than in mixed-ligand octaherdal complexes,[25,32,34,36,48,50,51] where the Cl ligand is located trans to N-donor moieties. In comparison with structurally characterized homoleptic $Fe^{III}(L)_2$ complexes,[55,63] the average Fe−N_{Ar} and the particular Fe−N_{ind} distances are longer in **3**, **4**, and **5** than those of the former (Table 3). A further difference is that the isoindoline ligands retain their planar structure, while in the homoleptic complexes ruffle- or saddle-shaped distortions have been often observed.[54−56]

Infrared spectroscopy can be informative about the coordination mode of the isoindoline-based ligands.[54−56] The neutral ligands with a hydrogen bound to an exocyclic amine nitrogen exhibit coupled C═N stretching vibrations above 1600 cm^{-1}. In contrast the corresponding vibrations in those that are anionic and have two exocyclic imine moieties are typically found between 1600 and 1500 cm^{-1}. The $FeCl_2(L^n)$ compounds all showed strong bands in the latter region that supports the anionic coordination mode. This way, in accordance with the determined structures, these complexes are neutral, with an iron(III) center surrounded by three anionic ligands.

Table 2. Selected Bond Distances (Å) and Angles (deg) for 3 and 5·$C_6H_5CH_3$

3		5·$C_6H_5CH_3$	
	Bond Distances (Å)		
Fe1−N1	2.019(2)	Fe1−N1	1.978(2)
Fe1−N3	2.094(2)	Fe1−N3	2.144(3)
Fe1−N5	2.095(2)	Fe1−N3A	2.143(3)
Fe1−Cl1	2.2216(8)	Fe1−Cl1	2.2284(10)
Fe1−Cl2	2.2344(8)	Fe1−Cl1A	2.2281(10)
	Bond Angles (deg)		
N1−Fe1−N3	86.01(9)	N1−Fe1−N3	86.66(10)
N3−Fe1−N5	171.29(9)	N3−Fe1−N3A	172.35(9)
Cl1−Fe1−Cl2	115.47(4)	Cl1−Fe1−Cl1A	114.43(4)
Cl1−Fe1−N1	117.42(7)	Cl1−Fe1−N1	120.15(8)

Table 3. Comparison of the Fe−N_{ind} and Fe−N_{Ar} Bond Distances (Å) of the Known Iron(III) Isoindoline Complexes

Ar-group of the ligand (complex)	Fe−N_{ind}	Fe−N_{Ar}	ref.
pyridine (**4**)	1.963(1)	2.148	57
4-methylpyridine (**5**)	1.978(2)	2.144	this work
thiazole (**3**)	2.019(2)	2.094	this work
thiazole ($[Fe^{III}(L^3)_2]^+$)	1.949	2.002	55
benzimidazole ($[Fe^{III}(L^1)^+]$)	1.928	1.978	63

In Situ Generation of the DBC^{2-}-Containing Model Complexes. To generate the [Fe(DBC)(L^n)] complexes (**1d**−**6d**), the commonly applied method of adding triethylamine to the mixture of the precursor complex and H_2DBC[24−51] in *N*,*N*-dimethylformamide (DMF) was followed. Upon addition of 2 equiv of base with respect to H_2DBC the color of the mixture changed to greenish-brown because of the presence of the typical catecholate-to-iron(III) charge-transfer band in the visible region that signals the displacement of chlorides with DBC^{2-}. (The intensity of the absorption band gradually increased and reached the maximum at 2 equiv of triethylamine upon titration. Adding more base up to 4 equiv did not yield further changes in the spectrum.) Importantly, it was shown earlier that one intense CT band is present at higher energy when HDBC$^-$ is coordinated as a monodentate ligand, whereas bidentate DBC^{2-} typically results in two CT bands, one that is higher (<500 nm) and one that is lower (>700 nm) in energy.[27] Energy shifts and intensities of the ligand-to-metal charge transfer (LMCT) bands depend on further factors, too, of which the Lewis-acidity of the iron(III) center and the symmetry of the iron-catecholate chelate are predominant.[38,41,42] In the case of our model complexes, **1d**−**6d** the low energy bands occur between 800 and 970 nm (Table 4) with very similar ε values. The second band at higher energy overlaps with the high intensity isoindoline-associated absorptions and therefore occurs as an ill-defined shoulder in

Table 4. Electrochemical and UV-vis Characteristics of the Complexes in DMF[a]

complex	$E^{\circ\prime}_{\mathrm{pa1}}$	$E^{\circ\prime}_{\mathrm{pa2}}$	$E^{\circ\prime}_{\mathrm{pc1}}$	$E^{\circ\prime}_{\mathrm{pc2}}$	$E^{\circ\prime}_{1/2}$	LMCT band $\lambda_{\max}$ (lg ε)
1	0.197		0.080		0.138	
2	0.229		0.128		0.179	
3	0.302		0.221	−0.173	0.262	
4	0.272			−0.233		
5	0.251		0.015	−0.352		
6	0.514		0.430	−0.045	0.472	
1d		0.305	−0.304			827 (3.43)
2d	0.150sh	0.324	−0.317			837 (3.43)
3d	0.260sh	0.430	−0.310			860 (3.38)
4d	0.270sh	0.432	−0.298			854 (3.48)
5d	0.270sh	0.439	−0.295			841 (3.49)
6d	0.235sh	0.400	−0.305			960 (3.40)

[a]Potentials are referenced against the Ag/AgCl reference electrode, $E^{\circ\prime}_{1/2}$ of ferrocene was 0.53 ± 0.01 V at 100 mV/s scan rate among identical conditions with the experiments.

Scheme 5. Designation of the Various Catecholate Adducts with **1**

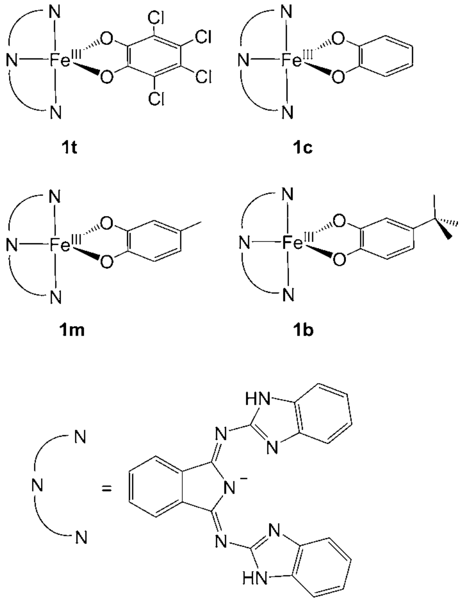

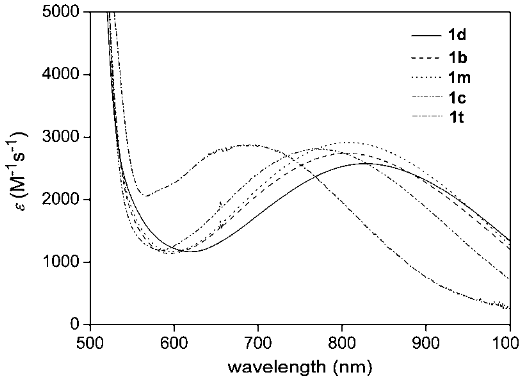

Figure 3. Lower energy catecholate to iron LMCT band for the various catecholate adducts with **1** (in DMF, at 25 °C, *c* = 1 mM, path length is 1 cm).

the spectra between ~460 and 510 nm. However, from the data it seems reasonable to propose that the complexes contain the substrate as a bidentate, dianionic ligand. It has been shown earlier that the LMCT band also shifts with changing the Lewis basicity of the catecholate ligand.[47] We used 3,4,5,6-tetrachlorocatechol (H_2TC), catechol (H_2CAT), 4-methylcatechol (H_2MC), and 4-*tert*-butylcatechol (H_2BC), for which the $E_{1/2}$ potentials are known,[47] (Table 5) to generate adducts with **1** (Scheme 5). In accordance with literature examples the wavelength of the catecholate to iron LMCT band is very sensitive to the substituents on the catecholate (Figure 3) and shows a correlation with the $E_{1/2}$ values (Figure 5a). Note that upon solvation the adducts may rearrange to six-coordinate species, but according to the spectroscopic data this would not affect the bidentate coordination mode of the substrate.

Electrochemistry. The catecholate to iron LMCT band shows variation with the Lewis basicity of the substrate (as it was demonstrated in Figure 3), and also does so with the type of the isoindoline ligand in the DBC^{2-}-containing complex series (Table 4). When the substrate is the same, the shift of the band can be associated with the change in Lewis acidity of the metal center that is induced by the ligand environment,[38] in our case the isoindoline-based ligands. For example, when the pyridyl pendant arms in **4d** are changed to more Lewis basic benzimidazole pendants in **1d** the LMCT energy becomes higher in accordance with expectations and literature findings.[26,36] To further elucidate the electronic effect of the different ligands, the redox properties of the precursor complexes **1**−**6** have been investigated by cyclic voltammetry (CV) experiments in DMF under Ar atmosphere, using 0.1 M TBAP as supporting electrolyte. The potential values for the observed anodic and cathodic current peaks ($E^{\circ\prime}_{\mathrm{pa}}$ and $E^{\circ\prime}_{pc}$) are listed in Table 4. Quasi-reversible, one-electron transitions are observed for **1**−**3** and **6** ($E^{\circ\prime}_{\mathrm{pa1}}$ and $E^{\circ\prime}_{\mathrm{pc1}}$), whereas **4** and **5** show irreversible waves ($E^{\circ\prime}_{\mathrm{pa1}}$, $E^{\circ\prime}_{\mathrm{pc1}}$, and $E^{\circ\prime}_{pc2}$, Figure 4) among experimental conditions. The peak separations for the quasi-reversible couples are somewhat larger than that of ferrocene (80 ± 5 mV). Furthermore, a second reduction wave is present by 0.37−0.47 V more negative potentials for **3**−**6** ($E^{\circ\prime}_{pc2}$) in the investigated potential range, indicating the presence of two electrochemically responsive species in

Table 5. Electrochemical Properties and LMCT Bands of the Catecholate Adducts of **1**[a]

complex	catechol	$E^{\circ\prime}_{\mathrm{pa}}$	$E^{\circ\prime}_{\mathrm{pc}}$	$E_{1/2}$[47] (H_2Cat/Q)	LMCT band $\lambda_{\max}$ (lg ε)	V_0 (10^{-8} M s^{-1})
1t	H_2TC	0.964	−0.484	0.312	690 (3.46)	n.r.
1c	H_2CAT	0.524	−0.092	−0.046	768 (3.45)	0.051
1m	H_2MC	0.465	−0.156	−0.123	802 (3.44)	0.084
1b	H_2BC			−0.142	808 (3.47)	0.373
1d	H_2DBC	0.305	−0.304	−0.222	827 (3.43)	61.1

[a]Potentials are referenced against the Ag/AgCl reference electrode, $E^{\circ\prime}_{1/2}$ of ferrocene was 0.53 V at 100 mV/s scan rate among identical conditions with the experiments.

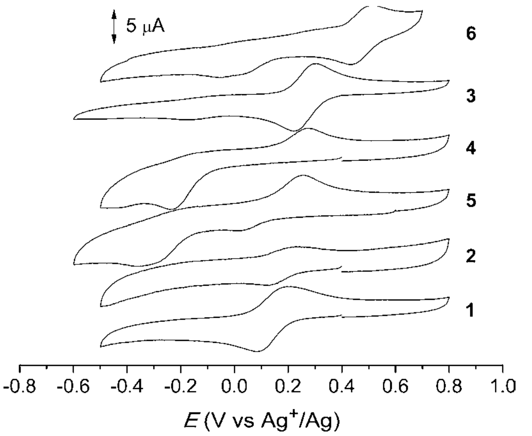

Figure 4. Cyclic voltammetry of complexes **1**–**6** in DMF at 25 °C (c = 1 mM).

solution. This may be attributed to chloride dissociation or exchange to solvent upon reduction because of the higher lability of the iron(II) species. Such behavior was reported for chloride complexes of iron(III) with tridentate ligands.[64] Therefore the couples (or the corresponding irreversible oxidations) at more positive potentials can be associated with the complexes that contain only one chloride while the more negative reduction waves with the $FeCl_2(L^n)$ precursors. Nevertheless, the potentials shift clearly with the applied ligand showing the same order as for the octahedral, $Fe(L^n)_2$ complexes[55] and other examples where 2-pyridyl, or 2-benzimidazolyl derivatives of the same ligand were studied.[26] More importantly, a correlation was found between the LMCT energy and the oxidation potential, $E^{\circ\prime}_{\rm pa1}$ of the iron center in the precursor complexes (Figure 5b). This indicates that the observed shift in the LMCT band of **1d**–**6d** can be attributed indirectly to the electronic effect of the isoindoline ligands.

It is remarkable that the slopes of the fitted lines in Figure 5a–b are almost equal with opposite direction (−5.27 cm^{-1} mV^{-1} for the ligand/iron(III) and 4.55 cm^{-1} mV^{-1} for the catecholate) representing the increasing energy gap between the metal-centered LUMO and the catecholate highest occupied molecular orbital (HOMO).

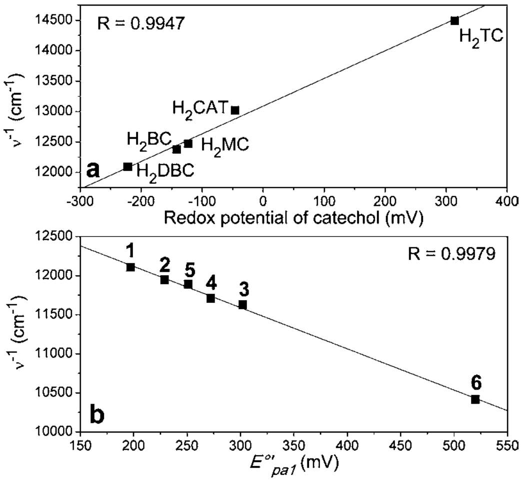

Figure 5. Correlation between the redox potential of the free catechols and the catecholate to iron LMCT energy of their adducts with **1** (a); correlation between the Fe(II)/Fe(III) oxidation potential of the precursor complexes **1**–**6** and the LMCT energy of the corresponding DBC^{2-} adducts **1d**–**6d** (b).

Upon addition of H_2DBC and triethylamine to the precursor complexes characteristic changes can be observed in the CVs (Figure 6). Instead of the quasi-reversible waves new, irreversible oxidations take place ($E^{\circ\prime}_{\rm pa2}$) that are sensitive to the isoindoline ligand. In all but one case (**1d**) shoulders are also present at somewhat lower potentials ($E^{\circ\prime}_{\rm pa1}$). On reduction irreversible current waves are present at very similar potentials ($E^{\circ\prime}_{\rm pc1}$) that can be associated with the $DBSQ^-$ to DBC^{2-} transition based on similar observations in the literature.[25,26,30,36] These transitions are at considerably higher potentials than that of free $DBSQ^-/DBC^{2-}$ couple (−1.43 V)[25] reflecting the significant stabilization of DBC^{2-} upon coordination to iron(III). Assignment of the oxidation features is vague in the CV of the DBC^{2-} adducts. However, we investigated the adducts of **1** with the different catechol-derivatives (**1m**, **1c**, and **1t**, Scheme 5) to decide whether the $E^{\circ\prime}_{\rm pa2}$ oxidation feature was sensitive to the catechol moiety. We found that the potential of the irreversible oxidation ($E^{\circ\prime}_{\rm pa}$ values in Table 5) shifted in the order **1t** > **1c** > **1m** > **1d** (Figure 7a) that corresponds the order in the LMCT energy (Figure 7b) and reactivity toward dioxygen (for data see Table 5). Therefore this feature can be attributed to the oxidation of the metal-bound catechol being sensitive to the isoindoline ligand in the **1d**–**6d** series.

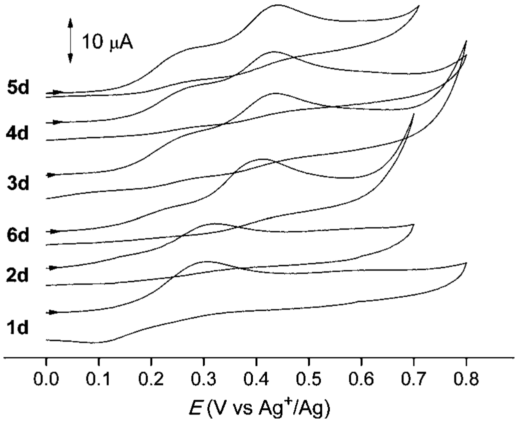

Figure 6. Cyclic voltammetry of the DBC^{2-} adducts **1d**–**6d** in DMF at 25 °C.

Reactivity of the DBC^{2-} Adducts. Products of the ring-cleaving reactions were identified by employing standard GC-MS method.[25,26,32,35,36,50,51] Solutions of the in situ detected substrate adduct complexes in DMF were exposed to dioxygen at 60 °C for 48 h and samples were analyzed by GC-MS. Scheme 6 shows the detected products, **A**–**F** that are consistent with the products reported in the literature.[25,26,32] Table 6 summarizes their relative abundance in the extracts. No attempt was made to separate the products, the isolated mixture of compounds was analyzed to estimate the intra- vs extradiol selectivity. Note that LC-MS measurements were also done to detect possible acidic components; however, these measurements only confirmed the GC-MS results.

From the data it can be concluded that reactions afford mainly the intradiol products (**A**–**C**), as it was expected for the meridional ligands used.[26,46] The extradiol lactones (**D** and **E**) were detected only in trace amounts and only one anhydride product was found (**F**) from other possible pathways[25,26,30–37]

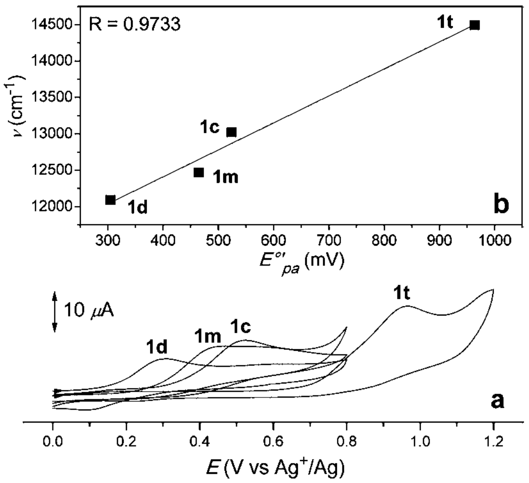

Figure 7. Cyclic voltammetry for the various catecholate adducts of **1** in DMF, at 25 °C (c = 1 mM) (a); correlation between the oxidation potential of the adducts and the energy of the catecholate to iron LMCT absorption band (b).

Scheme 6. Products of the Reactions between Complexes 1d–6d and Dioxygen: 3,5-di-*terc*-butyl-1-oxacyclohepta-3,5-diene-2,7-dione (A), 3,5-di-*terc*-butyl-5-(carboxymethyl)-2-furanone (B), 3,5-di-*terc*-butyl-1,6-bis(*N,N*-dimethylamino)-1,6-dione-2,4-hexadiene (C), 3,5-di-*terc*-butyl-2-pyrone (D), 4,6-di-*terc*-butyl-2-pyrone (E), and 3-*terc*-butyl-furan-2,5-dione (F)[36]

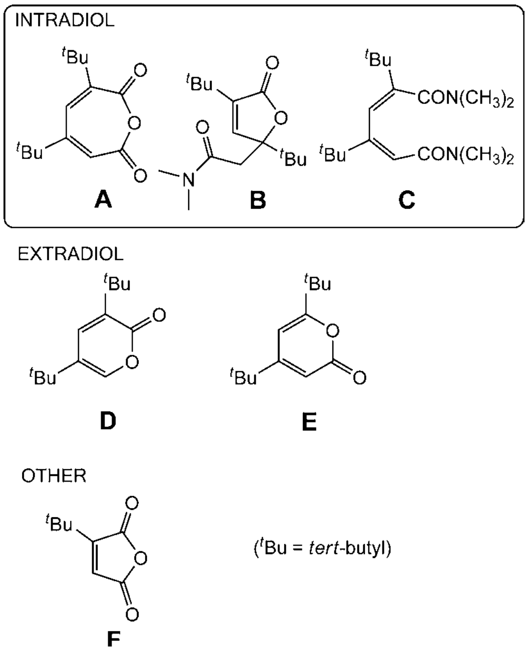

in detectable amount. In contrast with earlier reports on meridional ligands,[26,46] no quinone product was isolated. In Table 6 the estimated intra/extradiol (I/E) product ratios are also listed showing the highest selectivity in case of **1d** and **2d** and the lowest, but still considerable for **4d** and **5d**.

Kinetics of the dioxygenation reactions with the in situ generated DBC^{2-} adducts of **1**–**6** were investigated by UV–vis spectroscopy. Monitoring the change in the intensity of the lower energy LMCT band allows direct calculation of the adduct concentration. Figure 8 illustrates the typical spectral changes for **1d** during oxygenation and the actual concentration of **1d** (inset). The reactions were performed at different initial concentrations of **1d**–**6d**. In the case of the least reactive adduct, **5d**, the reaction performed by dissolving the isolated compound resulted in very similar initial reaction rate to that of the corresponding in situ experiment (Supporting Information, Figure S4). Therefore the in situ method was applied for the extended kinetics. The initial rate of the reaction shows good correlation with the initial concentration of the complexes (Figure 9) suggesting a first order dependence. In one case (**1d**) the initial reaction rates were measured at different dioxygen concentrations (Supporting Information, Figure S2). The data support first order dependence on dioxygen, thus the kinetic rate equation can be written as

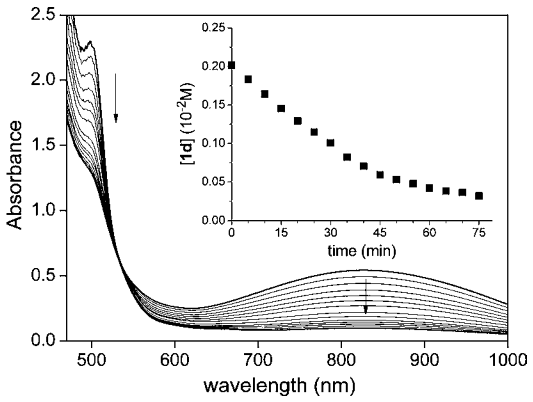

Figure 8. Changes in the electronic absorption spectrum with time during the reaction of **1d** with O_2 at 60 °C (Δt between the consecutive spectra is 5 min).

$$-\frac{d[\mathbf{1d}]}{dt} = k[\mathbf{1d}][O_2] \tag{1}$$

This equation can be accepted as the general rate equation for all complexes on the basis of their analogous properties. On the basis of the high I/E product ratios (6.5–46.5) and the minimal amount of other products (4% or less **F**) this equation can be associated dominantly with the intradiol pathway. The k values

Table 6. Detected Products (GC-MS) and Their Ratios from the Dioxygenation of Complexes 1d–6d

	intradiol products (%)			extradiol products (%)		other (%)	
complex	**A**, m/z = 236	**B**, m/z = 281	**C**, m/z = 309	**D**, m/z = 208	**E**, m/z = 208	**F**, m/z = 156	I/E ratio
1d	<1	33	60	~1	~1	2	46.5
2d	3	27	63	~1	~1	4	46.5
3d	4	53	26	3	3	4	13.8
4d	4	42	26	3	8	3	6.5
5d	8	42	33	7	6	2	6.4
6d	10	40	38	~1	3	4	22.0

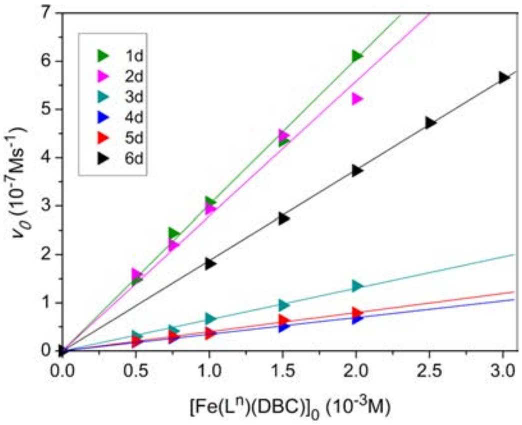

Figure 9. Dependence of the initial rates on the initial concentration of the adducts **1d**−**6d**.

Table 7. Average of Second Order Rate Constants[a] for the Reaction of Complexes 1d−6d[b]

complex	$k_{avg.}$ (10^{-2} M^{-1} s^{-1})
1d	24.6 ± 1.0
2d	23.6 ± 1.2
3d	5.02 ± 0.35
4d	2.90 ± 0.31
5d	3.19 ± 0.18
6d	15.0 ± 1.0

[a] Listed in Supporting Information, Tables S1−S6, experiments 1−5. [b] At 60 °C, concentration of dioxygen is 1.24 × 10^{-3} M.

and details of the kinetic studies are summarized in Supporting Information, Tables S1−S6 while Table 7 contains the averaged k values at 60 °C. The rates vary in the order, **1d** > **2d** > **6d** > **3d** > **4d** > **5d** that corresponds to the order in I/E selectivity. The temperature dependence of k was also investigated, the Eyring−Polanyi equation resulted in $\Delta H^{\ddagger}$ values in the range 49−56 kJmol^{-1} and $\Delta S^{\ddagger}$ values from −78 to −110 Jmol^{-1}K^{-1} (Supporting Information, Table S7) for the reactions.

Scheme 7. Proposed Mechanism for the Selective Intradiol Cleavage Reaction for Complexes 1d−6d

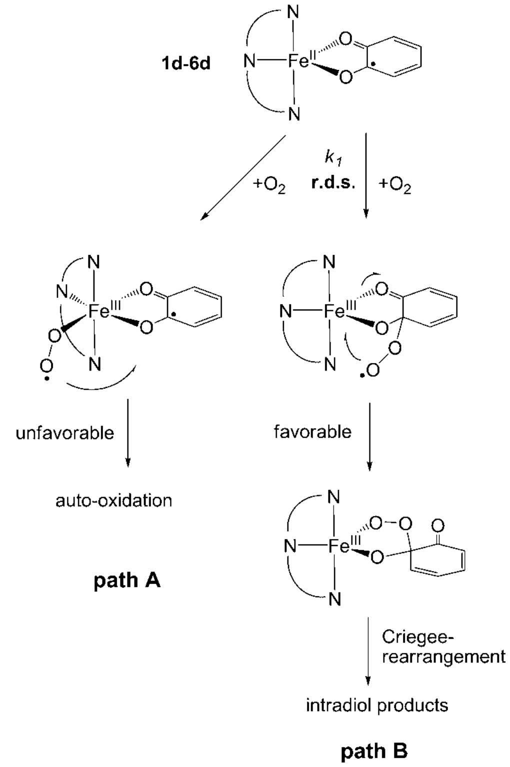

The presented observations allow us to draw a mechanism that is in accordance with the earlier proposed ones[26,36,46] (Scheme 7). The binding of the substrate that is facilitated by the high Lewis-acidity of the iron(III) center takes place instantly upon addition of triethylamine. The N_3 ligands, in general are good mimics for the metal binding site of the enzyme since three positions are available for substrate and dioxygen binding. In most precursor complexes three chlorides occupy these sites and after formation of the substrate adduct one chloride will still remain coordinated. In this respect our complexes are different, since only two chlorides are present in the precursors; thus, the in situ formed DBC^{2-} adduct will lack Cl$^-$. The attack of dioxygen may follow two pathways. Path A represents the situation when O_2 binds to the iron center. In the case of meridional ligands this means that the closure of the peroxide-bridge is disfavored because of steric constraints. Therefore the metal center merely "acts as a conduit for electrons from substrate to O_2" that is thought to generate the auto-oxidation product quinone as it was demonstrated with the terpy ligand.[46] Since this product was not observed in our system, path A should be negligible. Formation of the ring-cleaved products on the other hand implies that the reaction takes place and consequently should follow path B. This would mean that the attack of triplet dioxygen is favored at the substrate with semiquinone character. In the proposed mechanism this is thought to be the rate determining step (r.d.s.). The rate equation that can be delineated from this mechanism, $-d[\text{adduct}]/dt = k_1[\text{adduct}][O_2]$ is in accordance with the kinetic rate eq 1, if $k = k_1$. The considerable negative $\Delta S^{\ddagger}$ values may be also considered in support of an associative step for dioxygen attack. The meridional ligand geometry not only disfavors path A, but it can also be responsible for the high I/E selectivity. In the enzymatic reaction the intradiol selectivity is partly attributed to the planar geometry of the peroxo-bridged intermediate (Scheme 2) that leads to the Criegee-rearrangement.[23] Recently, density functional studies on an intradiol-cleaving model system with tetradentate ligand attributed intradiol-selectivity to the homolysis of the O−O bond.[65] On this basis the homolysis can be considered as an alternative for the Criegee-rearrangement for this system, too. Whichever is the situation, the intradiol selectivity can be reasonably attributed to the planar arrangement of peroxide oxygens and catecholate carbons because of steric constraints.[36,46] However, if the dioxygen attack takes place on the substrate, the reaction rate should be very sensitive to the type of the catecholate. This is indeed the case as the data in Table 5 illustrate. In addition, the LMCT energy vs $E^{\circ\prime}_{pa}$ correlation for the series **1d**, **1m**, **1c**, and **1t** shows very similar slope (3.71 ± 0.34 cm^{-1} mV^{-1}, Figure 7b) to that of the LMCT energy vs $E^{\circ\prime}_{1/2}$ of catechols (4.55 cm^{-1} mV^{-1}, Figure 5a) that may indicate significant catecholate character of the MO affected by this electrochemical oxidation. Finally, the logarithm of the rate constant k shows an inverse trend with the $E^{\circ\prime}_{pa2}$. This potential was attributed to the oxidation of the metal-bound catechol being sensitive to the isoindoline ligand in the **1d**−**6d** series; thus, the trend further supports the substrate activation mechanism (Figure 10). It also shows that the complexes with lower oxidation potential will react more rapidly with dioxygen as it can be expected.

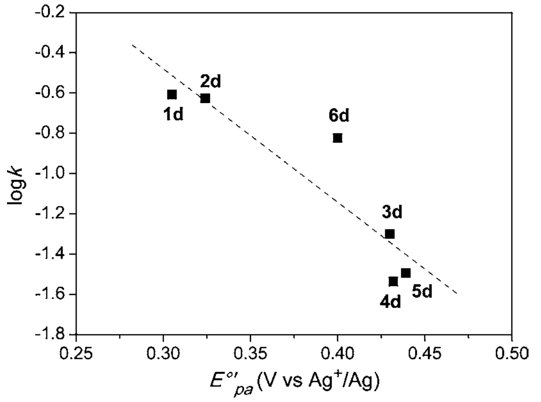

Figure 10. Change in the log *k* values with the $E^{\circ\prime}_{\mathrm{pa}}$ of the various model complexes ($R = 0.89$ for the fitted linear).

■ CONCLUSIONS

In this study six new catecholate adducts (**1d**−**6d**) have been investigated as models for the intradiol-cleaving catechol 1,2-dioxygenase enzymes. All ligands are isoindoline-based compounds (Scheme 4), monoanionic upon coordination to iron(III) and meridional by geometry that allowed an unprecedented scope of studies. Earlier, three models with meridional ligands (2,6-bis(2-pyridyl)pyridine: tpy; 2,6-bis(2-benzimidazolyl)pyridine: bbp; and pyridine-2,6-dicarboxylic acid: pda) have been compared by Palaniandavar and co-workers.[26] They associated the differences in reactivity with the Lewis acidity of the iron(III) center and the bulkiness of the bbp vs tpy ligand "hindering the fast approach of both catechol and dioxygen". They found a lower reaction rate paired with higher intradiol selectivity for the bbp ligand than for the tpy. This was quite in contrast with their earlier studies on *N,N*-bis(pyrid-2-ylmethyl)amine (bpa) and *N,N*-bis(benzimidazol-2ylmethyl)amine (bba). In this case they found much higher reactivity for the bulkier bba while the intradiol selectivity remained above 90% for both ligands[25] (they suggested "the N−H groups of the benzimidazole moieties to engage in H-bonding with the substrate-bound peroxo group" in the corresponding intermediate facilitating the intradiol pathway).

In our present study the different pendant-arms were able to tune the Lewis acidity of the iron(III) center as it could be judged from the electrochemical data for the precursor complexes **1**−**6**. The reaction rate and the I/E (intradiol over extradiol) selectivity followed the order of **1d** ~ **2d** > **6d** > **3d** > **4d** ~ **5d**; interestingly the bulkier ligands affording the better I/E selectivity and the higher reaction rates. Considering the very similar rates for the 1,3-bis-(2′-benzimidazolylimino)- and 1,3-bis-(*N*-methyl-2′-benzimidazolylimino)isoindoline containing adducts (**1d** and **2d**), the N−H groups are not likely to be involved in the reaction. Importantly, the *k* values for the dioxygenation reactions are dependent on the oxidation potentials for the adducts ($E^{\circ\prime}_{\mathrm{pa2}}$, Table 4, Figure 10). By comparing variously substituted catechols we could associate the $E^{\circ\prime}_{\mathrm{pa2}}$ with the coordinated catecholate. Therefore the log *k* vs potential plot in Figure 10 is in support of the substrate-activation mechanism. Finally, the decrease in I/E selectivity with the reaction rate in the **1d**−**6d** series suggests that the more these meridional ligands accelerate the reaction step leading to intradiol-cleavage the better the I/E selectivity is. It has been shown earlier that the attack of dioxygen at the iron(III) center leads to the auto-oxidation product quinone in case of meridional ligand geometry.[46] The absence of quinone from the product mixture shows that the attack of dioxygen at the iron is an unlikely event. On the other hand the presence of the extradiol-cleaved compounds may be associated with the different steric effects/flexibility of the isoindoline ligands[66] that allows geometric variations in the peroxo-bridged intermediate thus promoting the alkenyl- vs the acyl-migration of the proximal oxygen atom. This explanation would be in accordance with recent computational studies.[23,65]

■ ASSOCIATED CONTENT

Ⓢ Supporting Information

Crystallographic information files (CIF) for complexes **3** and **4**·$C_6H_5CH_3$, GC chromatogram for the product mixture from **1d** (Figure S1), dependence of the initial reaction rate of dioxygenation of **1d** on the dioxygen concentration (Figure S2), Eyring−Polanyi plots for the catecholate adducts **1d**−**6d** (Figure S3), electronic absorption spectrum of the in situ generated adduct **5d** (black) and the isolated complex (red) in DMF; insert: initial reaction rates for the oxygenation of the in situ generated adduct (black) and the isolated complex (red, for the experimental conditions see Table S5, exp. 5) (Figure S4), kinetic data for the dioxygenation of complexes **1d**−**6d** (Tables S1−S6) and corresponding activation parameters (Table S7). This material is available free of charge via the Internet at http://pubs.acs.org.

■ AUTHOR INFORMATION

Corresponding Author

*E-mail: kaizer@almos.vein.hu. Fax:+3688624469.

Notes

The authors declare no competing financial interest.

■ ACKNOWLEDGMENTS

The present article was published in the frame of the projects TÁMOP-4.2.1/B-09/1/KONV-2010-0003 and TÁMOP-4.2.2/B-10/1-2010-0025. The projects are realized with the support of the Hungarian Government and the European Union, with the co-funding of the European Social Fund. Furthermore, financial support of the Hungarian National Research Fund (OTKA K75783) and COST is also gratefully acknowledged. This project was supported by the János Bolyai research scholarship of the Hungarian Academy of Sciences.

■ REFERENCES

(1) Gibson, D. T. *Microbial Degradation of Organic Molecules*; Marcel Dekker: New York, 1984.

(2) Funabiki, T. *Oxygenases and Model Systems*; Kluwer: Dordrecht, The Netherlands, 1997.

(3) Costas, M.; Mehn, M. P.; Jensen, M. P.; Que, L., Jr. *Chem. Rev.* **2004**, *104*, 939.

(4) Parales, R.; Resnick, S. M. In *Biodegradation and Bioremediation*; Singh, A., Ward, O. P., Eds.; Springer: Heidelberg, Germany, 2004.

(5) Lipscomb, J. D.; Orville, A. M. Mechanistic Aspects of Dihydroxybenzoate Dioygenases. In *Metal Ions in Biological Systems*; Sigel, H., Sigel, I., Eds.; Marcel Dekker: New York, 1992; Vol. *28*, pp 243.

(6) Vaillancourt, F. H.; Bolin, J. T.; Eltis, L. D. *Crit. Rev. Biochem. Mol. Biol.* **2006**, *41*, 241.
(7) Ohlendorf, D. H.; Lipscomb, J. D.; Weber, P. C. *Nature* **1988**, *336*, 403.
(8) Valley, M. P.; Brown, C. K.; Burk, D. L.; Vetting, M. W.; Ohlendorf, D. H.; Lipscomb, J. D. *Biochemistry* **2005**, *44*, 11024.
(9) Pau, M. Y. M.; Davis, M. I.; Orville, A. M.; Lipscomb, J. D.; Solomon, E. I. *J. Am. Chem. Soc.* **2007**, *129*, 1944.
(10) Kita, A.; Kita, S. I.; Fujisawa, I.; Inaka, K.; Ishida, T.; Horiike, K.; Nozaki, M.; Miki, K. *Structure* **1999**, *7*, 25.
(11) Xin, M.; Bugg, T. D. H. *J. Am. Chem. Soc.* **2008**, *130*, 10422.
(12) Orville, A. M.; Lipscomb, J. D.; Ohlendorf, D. H. *Biochemistry* **1997**, *36*, 10052.
(13) Funabiki, T.; Yamazaki, T. *J. Mol. Catal. A: Chem* **1999**, *150*, 37.
(14) Bugg, T. D. H.; Ramaswamy, S. *Curr. Opin. Chem. Biol.* **2008**, *12*, 134.
(15) Christian, G. J.; Ye, S.; Neese, F. *Chem. Sci.* **2012**, *3*, 1600.
(16) Fielding, A. J.; Kovaleva, E. G.; Farquhar, E. R.; Lipscomb, J. D.; Que, L., Jr. *J. Biol. Inorg. Chem.* **2011**, *16*, 341.
(17) Gunderson, W. A.; Zatsman, A. I.; Emerson, J. P.; Farquhar, E. R.; Que, L., Jr.; Lipscomb, J. D.; Hendrich, M. P. *J. Am. Chem. Soc.* **2008**, *130*, 14465.
(18) Mbughuni, M. M.; Chakrabarti, M.; Hayden, J. A.; Bominaar, E. L.; Hendrich, M. P.; Münck, E.; Lipscomb, J. D. *Proc. Natl. Acad. Sci.U.S.A.* **2010**, *107*, 16788.
(19) Fielding, A. J.; Lipscomb, J. D.; Que, L., Jr. *J. Am. Chem. Soc.* **2012**, *134*, 796.
(20) Kovaleva, E. G.; Lipscomb, J. D. *Science* **2007**, *316*, 453.
(21) Mendel, S.; Arndt, A.; Bugg, T. D. H. *Biochemistry* **2004**, *43*, 13390.
(22) Lipscomb, J. D. *Curr. Opin. Struct. Biol.* **2008**, *18*, 644.
(23) Borowski, T.; Siegbahn, P. E. M. *J. Am. Chem. Soc.* **2006**, *128*, 12941.
(24) Yamahara, R.; Ogo, S.; Masuda, H.; Watanabe, Y. *J. Inorg. Biochem.* **2002**, *88*, 284.
(25) Velusamy, M.; Mayilmurugan, R.; Palaniandavar, M. *J. Inorg. Biochem.* **2005**, *99*, 1032.
(26) Dhanalakshmi, T.; Bhuvaneshwari, M.; Palaniandavar, M. *J. Inorg. Biochem.* **2006**, *100*, 1527.
(27) Mayilmurugan, R.; Suresh, E.; Palaniandavar, M. *Inorg. Chem.* **2007**, *46*, 6038.
(28) Li, F.; Wang, M.; Li, P.; Zhang, T.; Sun, L. *Inorg. Chem.* **2007**, *46*, 9364.
(29) Wang, C.-H.; Lu, J.-W.; Wei, H.-H.; Takeda, M. *Inorg. Chim. Acta* **2007**, *360*, 2944.
(30) Mayilmurugan, R.; Stoeckli-Evans, H.; Palaniandavar, M. *Inorg. Chem.* **2008**, *47*, 6645.
(31) Mayilmurugan, R.; Visvaganesan, K.; Suresh, E.; Palaniandavar, M. *Inorg. Chem.* **2009**, *48*, 8771.
(32) Sundaravel, K.; Suresh, E.; Palaniandavar, M. *Inorg. Chim. Acta* **2010**, *363*, 2768.
(33) Paria, S.; Halder, P.; Paine, T. K. *Inorg. Chem.* **2010**, *49*, 4518.
(34) Mayilmurugan, R.; Sankaralingam, M.; Suresh, E.; Palaniandavar, M. *Dalton Trans.* **2010**, *39*, 9611.
(35) Visvaganesan, K.; Ramachitra, S.; Palaniandavar, M. *Inorg. Chim. Acta* **2011**, *378*, 87.
(36) Anitha, N.; Palaniandavar, M. *Dalton Trans.* **2011**, *40*, 1888.
(37) Sundaravel, K.; Suresh, E.; Saminathan, K.; Palaniandavar, M. *Dalton Trans.* **2011**, *40*, 8092.
(38) Cox, D. D.; Benkovic, S. J.; Bloom, L. M.; Bradley, F. C.; Nelson, M. J.; Que, L., Jr.; Wallick, D. E. *J. Am. Chem. Soc.* **1988**, *110*, 2026.
(39) Hitomi, Y.; Yoshida, M.; Higuchi, M.; Minami, H.; Tanaka, T.; Funabiki, T. *J. Inorg. Biochem.* **2005**, *99*, 755.
(40) Jo, D.-H.; Chiou, Y.-M.; Que, L., Jr. *Inorg. Chem.* **2001**, *40*, 3181.
(41) Mialane, P.; Tchertanova, L.; Banse, F.; Sainton, J.; Girerd, J.-J. *Inorg. Chem.* **2000**, *39*, 2440.
(42) Raffard, N.; Carina, R.; Simaan, A. J.; Sainton, J.; Riviére, E.; Tchertanova, L.; Bourcier, S.; Bouchoux, G.; Delroisse, M.; Banse, F.; Girerd, J.-J. *Eur. J. Inorg. Chem.* **2001**, 2249.
(43) Velusamy, M.; Mayilmurugan, R.; Palaniandavar, M. *Inorg. Chem.* **2004**, *43*, 6284.
(44) Higuchi, M.; Hitomi, Y.; Minami, H.; Tanaka, T.; Funabiki, T. *Inorg. Chem.* **2005**, *44*, 8810.
(45) Funabiki, T.; Yamazaki, T.; Fukui, A.; Tanaka, T.; Yoshida, S. *Angew. Chem., Int. Ed.* **1998**, *37*, 512.
(46) Jo, D.-H.; Que, L., Jr. *Angew. Chem., Int. Ed.* **2000**, *39*, 4284.
(47) Pascaly, M.; Duda, M.; Schweppe, F.; Zurlinden, K.; Müller, F. M.; Krebs, B. *J. Chem. Soc., Dalton Trans.* **2001**, 828.
(48) Yoon, S.; Lee, H.-J.; Lee, K.-B.; Jang, H. G. *Bull. Korean Chem. Soc.* **2000**, *21*, 923.
(49) Ogihara, T.; Hikichi, S.; Akita, M.; Moro-oka, Y. *Inorg. Chem.* **1998**, *37*, 2614.
(50) Visvaganesan, K.; Mayilmurugan, R.; Suresh, E.; Palainandavar, M. *Inorg. Chem.* **2007**, *46*, 10294.
(51) Sundaravel, K.; Dhanalakshimi, T.; Suresh, E.; Palainandavar, M. *Dalton Trans.* **2008**, 7012.
(52) Kaizer, J.; Kripli, B.; Speier, G.; Párkányi, L. *Polyhedron* **2009**, *28*, 933.
(53) Pap, J. S.; Kaizer, J.; Speier, G. *Coord. Chem. Rev.* **2010**, *254*, 781.
(54) Pap, J. S.; Kripli, B.; Giorgi, M.; Kaizer, J.; Speier, G. *J. Inorg. Biochem.* **2011**, *105*, 911.
(55) Kripli, B.; Baráth, G.; Balogh-Hergovich, É.; Giorgi, M.; Simaan, A. J.; Párkányi, L.; Pap, J. S.; Kaizer, J.; Speier, G. *Inorg. Chem. Commun.* **2011**, *14*, 205.
(56) Pap, J. S.; Kripli, B.; Bányai, V.; Giorgi, M.; Korecz, L.; Gajda, T.; Árus, D.; Kaizer, J.; Speier, G. *Inorg. Chim. Acta* **2011**, *376*, 158.
(57) Balogh-Hergovich, É.; Speier, G.; Tapodi, B.; Reglier, M.; Michel, G. *Z. Kristallogr. NCS* **1999**, *214*, 579.
(58) Siegl, W. O. *J. Org. Chem.* **1977**, *42*, 1872.
(59) Siggelkow, B.; Meder, M. B.; Galka, C. H.; Gade, L. H. *Eur. J. Inorg. Chem.* **2004**, *761*, 3424.
(60) Sheldrick, G. M. *Acta Crystallogr.* **2008**, *A64*, 112.
(61) Burla, M. C.; Caliandro, R.; Camalli, M.; Carrozzini, B.; Cascarano, G. L.; De Caro, L.; Giacovazzo, C.; Polidori, G.; Spagna, R. *J. Appl. Crystallogr.* **2005**, *38*, 381.
(62) Addison, A. W.; Rao, T. N.; Reedijk, J.; van Rijn, J.; Verschoor, G. C. *J. Chem. Soc., Dalton Trans.* **1984**, 1349.
(63) Pap, J. S.; Giorgi, M.; Kaizer, J.; Speier, G. *Inorg. Chem. Commun.* **2013**, *27*, 152.
(64) Rodriguez, M.-C.; Morgensern-Badarau, I.; Cesario, M.; Guilhem, J.; Keita, B.; Nadjo, L. *Inorg. Chem.* **1996**, *35*, 7804.
(65) Georgiev, V.; Noack, H.; Borowski, T.; Blomberg, M. R. A.; Siegbahn, P. E. M. *J. Phys. Chem. B* **2010**, *114*, 5878.
(66) J. S. Pap, J. S.; Bányai, V.; Szilvási, D. S.; Kaizer, J.; Speier, G.; Giorgi, M. *Inorg. Chem. Commun.* **2011**, *14*, 1767.